THE ASTRONOMICAL JOURNAL VOLUME 108, NUMBER 3 SEPTEMBER 1994

STRUCTURE AND PROPER MOTIONS IN HERBIG–HARO OBJECTS 1 AND 2

JOCHEN EISLÖFFEL
Dublin Institute for Advanced Studies, School of Cosmic Physics, 5 Merrion Square, Dublin 2, Ireland

REINHARD MUNDT
Max-Planck-Institut für Astronomie, Königstuhl 17, D-69117 Heidelberg, Germany

KARL-HEINZ BÖHM
Astronomy Department, FM-20, University of Washington, Seattle, Washington 98195

Received 1994 March 1; revised 1994 April 26

ABSTRACT

We have carried out a detailed study on the structure and proper motions of the condensations in Herbig–Haro (HH) objects 1 and 2 and other HH objects in their immediate neighborhood. The presented proper motions are compatible with HH 1 being a bow shock, which is propagating into a moving medium ahead of it. They also reveal a very complex kinematical structure in HH 2. Proper motions for the nearby HH objects HH 144, HH 145, and the newly discovered HH 147 are presented and the probable outflow sources for HH 144 and HH 147 are identified. Tangential velocities in the range of 100–250 km s^{-1} were measured for the condensations in HH 2, HH 144, and HH 147, while velocities of up to 380 km s^{-1} were found in the HH 1 bow shock and in the jet pointing from the VLA1 source towards HH 1 (VLA1 jet). These outflows appear not to be well aligned with respect to each other, nor with the local cloud magnetic field. Linear correlations between tangential velocities and excitation and radial velocity dispersion, respectively, were found for condensations in HH 1 and 2. Surprisingly an anticorrelation between tangential velocity and radial velocity dispersion was found in the VLA1 jet. A deconvolved [S II] image of HH 1 (FWHM=0.″55) shows a wealth of structural details in the bow shock and (just) resolves the knots in the VLA1 jet, whose diameter could be measured. The deconvolved [S II] image, as well as an Hα image and the low tangential velocity suggest, that knot G_J might consist of two closely spaced components, one of which is excited by the entrainment of ambient material into the VLA1 jet. Photometric monitoring between 1987 and 1993 shows that many of the brighter condensation in HH 1 and 2 were variable in the [S II]$\lambda\lambda$ 6716,6731 lines. Most notable are the brightening of HH 2H by about 25%, the fading of HH 2C and G by about 20% and the strong variability of 10%–30% within only six years found for HH 1G, HH 2A′, B, D, and G.

1. INTRODUCTION

Since their discovery by Herbig (1951) and Haro (1952) the HH objects 1 and 2 have been the subject of numerous studies at various wavelength regions. Among the most important investigations for understanding this outflow system were probably the proper motion studies by Herbig & Jones (1981) and the VLA radio continuum observations by Pravdo *et al.* (1985). These two studies showed that HH 1 and HH 2 are moving away in opposite directions from the deeply embedded source VLA1 at speeds of up to about 350 km s^{-1}. Before the Pravdo *et al.* (1985) observations it was thought that the faint T Tauri star (TTS) 25″ southeast of HH 1, better known as the Cohen–Schwartz (CS) star, would be the exciting star (Cohen & Schwartz 1979). The deeply embedded source VLA1 illuminates a biconical reflection nebula, which is located on the axis of the HH 1/2 outflow (e.g., Strom *et al.* 1985). The nature of this radio source is unknown, but its luminosity of about 50 $L_\odot$ (Harvey *et al.* 1986) is typical for a high-luminosity TTS.

Various CCD imaging studies (e.g., Strom *et al.* 1985; Mundt *et al.* 1987) showed that a low-excitation emission-line jet is pointing from VLA1 towards HH 1, which, like several other HH objects, has the shape of a bow shock. This morphology is rather similar to the one observed for HH 34 and its jet (see, e.g., Bührke *et al.* 1988). No counterjet pointing towards HH 2 has been found so far; only the recent $H_2v=1$-0 $S(1)$ 2.12 μm images of Davis *et al.* (1994) give some hints in this direction. In their H_2 images the VLA1 jet is relatively prominent, which is not surprising in consideration of the low excitation observed at optical wavelengths. Since HH 1 and HH 2 both have rather small radial velocities ($\leqslant$10–40 km s^{-1}) their spatial motions are very close to plane of the sky, which might also explain why no associated bipolar molecular flow has been discovered so far (Edwards & Snell 1984).

Both HH 1 and HH 2 have been studied in detail by long-slit spectroscopy (e.g., Choe *et al.* 1985; Raga *et al.* 1988; Solf *et al.* 1991) which revealed their rather complex physical structure. These studies strongly support the idea that HH 1 is indeed a bow shock driven by a high-velocity jet and moving into a medium ahead of HH 1, which is already moving itself. For HH 2, however, the basic flow structure could not yet be clarified. This object appears to be a complex conglomerate of condensations, which might result from a counter bow shock and which, for yet unknown reasons (e.g., instabilities, variability of the source), has fragmented into many "clumps" (see also Raga *et al.* 1988). The

 0004-6256/94/108(3)/1042/14/$0.90

TABLE 1. Log of CCD images.

Date	Filter	Exp. time	Telescope
1986 Nov 22	[SII]	2×1500 s	KPNO 2.1m
1987 Jan 4	[SII]	1400 s	Calar Alto 3.5m
1987 Jan 4	Hα	1200 s	Calar Alto 3.5m
1987 Jan 6	[OIII]	1400 s	Calar Alto 3.5m
1988 Dec 12	[SII]	1600 s	Calar Alto 3.5m
1990 Nov 18	[SII]	1800 s	Calar Alto 3.5m
1990 Nov 19	[SII]	2400 s	Calar Alto 3.5m
1991 Feb 9	[SII]	1200 s	ESO NTT 3.5m
1992 Jan 3	[SII]	2700 s	ESO/MPI 2.2m
1992 May 2	[SII]	2300 s	ESO/MPI 2.2m
1993 Apr 1	[SII]	2400 s	ESO/MPI 2.2m

high-resolution images of HH 2 obtained recently with the Hubble Space Telescope (Schwartz *et al.* 1993) also confirmed the complex morphological structure of this object. More recent observations by Reipurth *et al.* (1993) showed that HH 1 and 2 do not trace the only outflow in this region, but that there is an additional source (called VLA2) about 3″ southeast of VLA1, which probably drives the collimated flow HH 144 towards the west. Two other faint HH objects were found further west (HH 145) and southwest (HH 146), respectively.

In this paper we show that the whole situation is even more complex and that at least four HH flows are present in the region of HH 1/2. The main aim of this paper, however, is the investigation of the kinematical structure of HH 1, HH 2, and the VLA1 jet with the help of proper motion measurements based on emission-line CCD images. Compared to the first photographic proper motion study by Herbig & Jones (1981) our new CCD-based study allowed us to investigate many of the faint knots and a total of 56 knots were measured, while it was only 12 knots in the work of Herbig & Jones (1981). Additionally we present proper motion measurements for condensations in HH 144, HH 145, and HH 147. With our CCD images it was also possible to study the photometric variability of the knots in HH 1 and HH 2 over the past six years and a deconvolution of a [S II]λλ 6716, 6731 image revealed interesting structural details in the region between VLA1 and HH 1.

2. OBSERVATIONS AND DATA REDUCTION

Our proper motion measurements are based on nine [S II]λλ 6716, 6731 narrow-band CCD images taken at various telescopes (Table 1). All frames used for this investigation were taken between 1986 November and 1992 May, i.e., with a total epoch difference of $5\frac{1}{2}$ years. Seeing conditions were not always favorable. Seeing varied between 1.″0 and 2.″0, with a mean of 1.″5 (FWHM). The data reduction and the proper motion measurements of the individual knots and condensations were carried out as described by Eislöffel & Mundt (1992). In that paper we also described how we dealt with the so-called "virtual" knots. In the original frames they usually do not show up as local maxima, but as regions of flat or less steep intensity gradients. In images of higher spatial resolution these virtual knots normally become local maxima, i.e., real knots [compare, e.g., knot HH 1B in Figs. 2 and 5(a)]. Usually the virtual knots show somewhat, but not much larger measurement errors than do isolated knots of comparable brightness. For the sake of simplicity we will refer to virtual knots as knots throughout this paper.

In 1987 January two additional CCD images were taken through narrow-band filters centered on Hα (λ_c=6580 Å, FWHM=100 Å) and the [O III]λλ4959, 5007 lines (λ_c=4990 Å, FWHM=100 Å). They were both taken under a seeing of 1.″0.

In addition to the proper motion study we also deconvolved HH 1 and the VLA1 jet on the [S II] image, which was taken on 1990 November 19 under a seeing of 1.″1 (FWHM) and which had the highest S/N ratio. The deconvolution was done with the help of the Richardson–Lucy algorithm. For the image shown in this paper we stopped the deconvolution process after 40 iteration steps, because after 50 to 70 steps weak artefacts tended to show up. The resulting image has a resolution of 0.″55 (FWHM) as measured from field stars.

Furthermore we did photometry of the brighter condensations in HH 1/2 on the seven [S II] CCD images taken at the Calar Alto 3.5 m and the ESO/MPI 2.2 m telescopes between 1987 January and 1993 April. This helps us to judge whether in some cases the apparent proper motion may be influenced by brightness changes. A 5″ aperture was centered on the condensations and about 0.″3 (about one pixel) away in all cardinal directions to estimate the influence of variable seeing and neighboring condensations. The sky was measured at fixed positions away from the HH objects. Two stars, Nos. 4 and 6 of Strom *et al.* (1985), which were present on all our images, were used as reference. They were found to be nonvariable during our monitoring period with respect to each other and relative to other stars not present in all our images, and also in the photometry carried out by Strom *et al.* (1985) in 1984 November.

3. RESULTS

An overview over the whole region around the HH 1/2 system is given on the deep [S II] image shown in Fig. 1 [Plate 28], which was taken at the ESO/MPI 2.2 m telescope in 1992 May. The whole, rather complex region consists of at least four HH flows and the properties of the individual flows will be discussed in detail below. The brightest and most prominent objects in the field are HH 1 and HH 2. A well-collimated jet is located northwest of the embedded source VLA1 and is pointing towards HH 1 (Strom *et al.* 1985). North of this VLA1 jet and southeast of the CS star some

patchy HH condensations are visible. West of the VLA1 jet a chain of mostly faint knots, called HH 144, points westwards and apparently ends in a region of several more diffuse, faint knots, called HH 145 (Reipurth *et al.* 1993). Northeast of HH 1 there are two more diffuse HH knots, which do not seem to belong to any of the other known HH objects in this region. We therefore call them HH 147. Furthermore, in the upper-right-hand corner of our image some faint knots are visible, which are believed to belong to HH 3 (Reipurth 1989). In the following we present high-resolution imaging of HH 1, photometry of condensations in HH 1 and 2, and proper motions for the various HH objects in this field (with the exception of the knots thought to belong to HH 3).

3.1 High-Resolution Imaging of HH 1

Figure 2 [Plate 29] shows our deconvolved image of the region between VLA1 and HH 1. An enlarged contour plot in the inset of Fig. 2 shows the HH 1 bow shock in more detail. The deconvolved image has a resolution of 0.″55 (FWHM) as measured from field stars. A comparison with the original image shows that apparently "new" features and knots are already suggested in the original image as extensions or "shoulders" of neighboring brighter knots. For an original image the reader is referred to Fig. 5(a) (see below). There also the designations for the knots in the VLA1 jet are given.

In the deconvolved image the knots of the VLA1 jet stand out as clearly separated features. They are not perfectly aligned, however; e.g., both knot B_J and E_J are displaced to the southwest relative to a line drawn through knots C_J, D_J, and F_J. Knot G_J, the one closest to the source, has an extraordinary shape. It is elongated with its major axis more or less perpendicular to the jet axis. While its brightest part is well aligned with the other knots in the jet, a major fraction of the [S II] emission comes from a region off the jet axis. In our Hα image (not shown here) the off-axis part of knot G_J is much brighter than the on-axis part. This suggests that knot G_J might be a feature consisting of an on-axis jet knot of lower excitation and a very nearby off-axis knot of clearly higher excitation. Such regions of higher excitation along the border of the jet have recently been found in the HH 46/47 jet by Hartigan *et al.* (1993). In these regions also lower radial velocities (Hartigan *et al.* 1993) and lower tangential velocities (Eislöffel & Mundt 1994) were measured. The formation of these knots in HH 46/47 has been attributed to entrainment of ambient material into the jet channel. The similar morphology and excitation of knot G_J suggests, that its outer part may as well result from strong shocks in gas entrained into the jet. Further indirect evidence for entrainment near knot G_J is also provided by its relatively large radial velocity dispersion (see Sec. *4.3.3*).

We fitted a two-dimensional Gaussian profile across each single jet knot in the deconvolved image and computed the diameter of the knots taking the width of the point-spread function into account. Our results are given in Fig. 3 in a plot of jet half-diameter (HWHM) against distance from the source. We find that in our deconvolved image the jet knots are just resolved (some only marginally). At knot G_J the visible part of the jet starts with a diameter of 1.″0, which

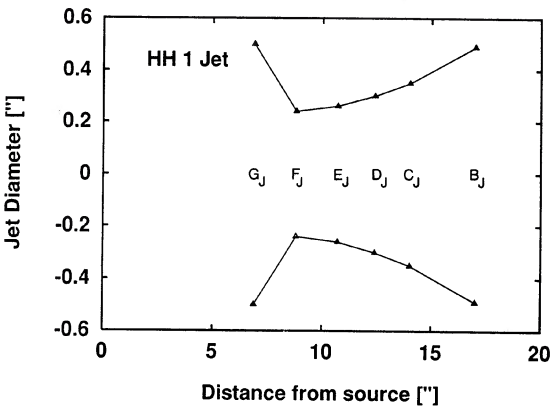

FIG. 3. Jet diameter of the VLA1 jet as a function of distance from the source. After its initial convergence between knots G_J (which probably consists of two laterally closely spaced knots) and F_J the opening angle of the VLA1 jet increases outward to knot B_J at about 3° on average.

decreases to half this value at knot F_J, again demonstrating the extraordinary shape of knot G_J. From knot F_J out to knot B_J the jet diameter and the jet opening angle increase steadily; while the full opening angle between knots F_J and E_J is about 1°, it expands to about 5° between knots C_J and B_J. The average full opening angle along the visible part of the jet between knots F_J and B_J is found to be about 3°. These values are in the same range as observed in other jets (Mundt *et al.* 1991; Raga *et al.* 1991). Most of the 15 jets investigated by these authors showed, however, a constant or decreasing opening angle with increasing distance from the source. "Flaring" of the jet diameter, as in the case of the VLA1 jet, was only observed for the HH 34 jet at similar distances from the source. If we left out the measurement for the unusual knot G_J for a moment and extrapolated the jet diameter back to the source, we would end up with a jet diameter at the source of about 0.″4. This value is four times larger than the upper limit for the diameter of $\leq$0.″1 at the position of VLA1 derived by Rodríguez *et al.* (1990) from VLA observations at 2 cm. This means that the full opening angle of the jet between the VLA1 source and the first visible knot F_J has to be larger (more than 2.″5 on average) than it is between knots F_J and E_J (where we measured an angle of about 1°). This behavior is reminiscent of several of the jets observed by Mundt *et al.* (1991), Raga *et al.* (1991), and Hirth *et al.* (1994) where there is indirect evidence that the jet opening angles are much larger close to the source.

In the deconvolved image the bow shock structure of HH 1 becomes more evident as several of the known knots split up (see inset in Fig. 2). Especially the northeastern bright part of the bow shock shows a wealth of detail. Knots *D* and *E* show up as isolated knots and between *D* and *F* a further knot is indicated. A similar situation occurs for knot *B*. This knot is now seen isolated in the deconvolved image and a new one appears between it and the bright knot *F*. Further away from the apex of the bow shock, knot *C* appears well separated from *A* and between knots *A* and *K* and *A* and *L*, respectively, previously unseen features shows up. The outer boundary of the bow shock does no longer look smooth,

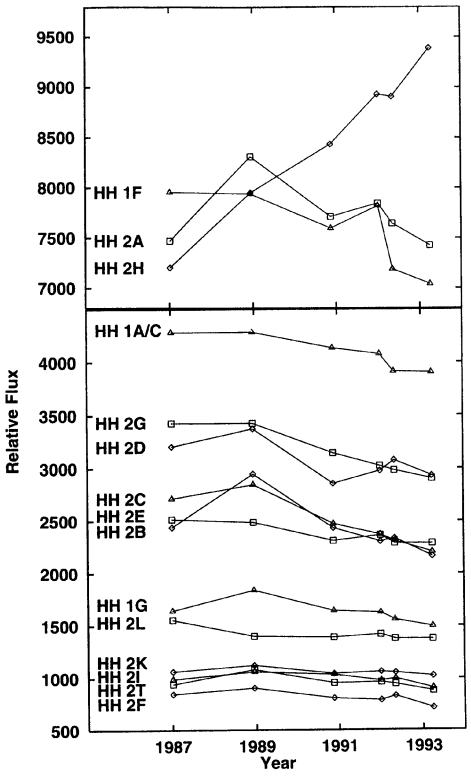

FIG. 4. Relative photometry of condensations on HH 1 and 2 in the [S II]λλ 6716, 6731 lines. The fluxes are normalized to star No. 6 of Strom *et al.* (1985) and are accurate to better than ±2% on average. The measurements from two consecutive nights in 1990 November have been averaged for clarity. Most knots show variability of 10%–30%.

especially at its northeastern bright edge, but becomes "bumpy." Rather than a smooth parabola, a row of bright clumps forms the outer edge of the bow shock. This resembles very much the appearance of the bow shock in the numerical simulations of radiatively cooling jets (e.g., Blondin *et al.* 1989; Blondin *et al.* 1990). In these simulations shocked gas can condense to a dense cold shell at the head of the jet, which eventually becomes unstable and fragments into distinct clumps. Such bumpy edges are also indicated in a few other HH objects with shapes of bow shocks. Notable examples are RNO 43S (Mundt *et al.* 1987) and HH 45 (Reipurth 1989).

The deconvolved image also contains the first two knots of the HH 144 outflow, HH 144A and B. Knot HH 144B is clearly resolved into two knots now.

3.2 Photometry of Condensations in HH 1 and HH 2

In order to investigate brightness variations of the condensations in HH 1 and 2 in more detail we carried out relative photometry for the brighter condensations in our [S II] CCD images. In Fig. 4 we present the relative brightness of the measured condensations normalized to star No. 6 of Strom *et al.* (1985). A comparison of measurements from two consecutive nights in 1990 November (which were averaged in Fig. 4 for clarity) shows that our measurement errors are well below ±2% on average.

In HH 1 we measured the three knots A/C, G, and F. Note that when we measured knot A our 5″ aperture included almost all of the nearby condensation C. We find that all three knots have faded by about 10%. Condensation G furthermore exhibited a variability of about 20% during our monitoring period. The fading of knot A/C continues now for over three decades, since it was observed already in 1959 by Herbig & Jones (1981). For knot F they found a considerable brightening during the 1960s and 1970s. This trend seems to have stopped (and possibly reversed) in the meantime.

In HH 2 we measured the twelve knots A', B, C, D, E, F, G, H, I, K, L, and T [for designations see Fig. 6(a)]. We find that knots B, E, and L faded at a 10% level, while knots C and G showed an even stronger fading of about 20%. Knot H brightened strongly by about 25% and is now clearly the brightest knot in the whole HH 1/2 system. A number of knots (A',B,D,G) exhibited substantial variability of 10%–30% during a time interval as short as 6 yr (our monitoring period). Condensation HH 2G, which newly appeared at about the same time in the early 1950s as HH 2H (see below) and was equally bright around 1960, is fading again, in contrary to the latter knot, and is already about 1.3 mag fainter by now. Only condensations F, I, and K were found to be stable within their measurement errors.

Herbig (1969) and Herbig & Jones (1981) have reported variability for a number of knots in HH 2 between 1946 and 1981: most surprisingly two new knots, H and G, appeared in the early 1950s after brightening by more than 2 mag within less than 5 yr. Knots C and G were found slightly variable since the mid-1950s, while several others were fading (knot A since the mid-1950s, B since the mid-1940s, and D during the 1960s and 1970s). A new knot named A' appeared about 1″ north of the original knot A during the late 1950s and is dominating the light of this condensation since then.

Although changes in the shape of individual condensations were not noticed during the time span of our observations, both processes, brightening and fading of condensations, might have some influence on our proper motion measurements, which are presented in the next sections.

3.3 Proper Motion Measurements of HH 1

The designations of the individual knots in HH 1, in the region southeast of the CS star and in the VLA1 jet are given in Fig. 5(a). For the HH 1 bow shock we adopted the designations by Herbig & Jones (1981) and extended them according to our needs. For the VLA1 jet we adopted the designations by Reipurth *et al.* (1993). Table 2 gives the proper motions for all measured knots in HH 1, southeast of the CS star and in the VLA1 jet. Table 2 lists the proper motions (in ″/yr) and the tangential velocities (in km s^{-1}) for an assumed distance to HH 1/2 of 450 pc, as well as the position angles of the proper motion vectors (in degrees). Figure 5(b) shows the proper motion vectors for all of these knots.

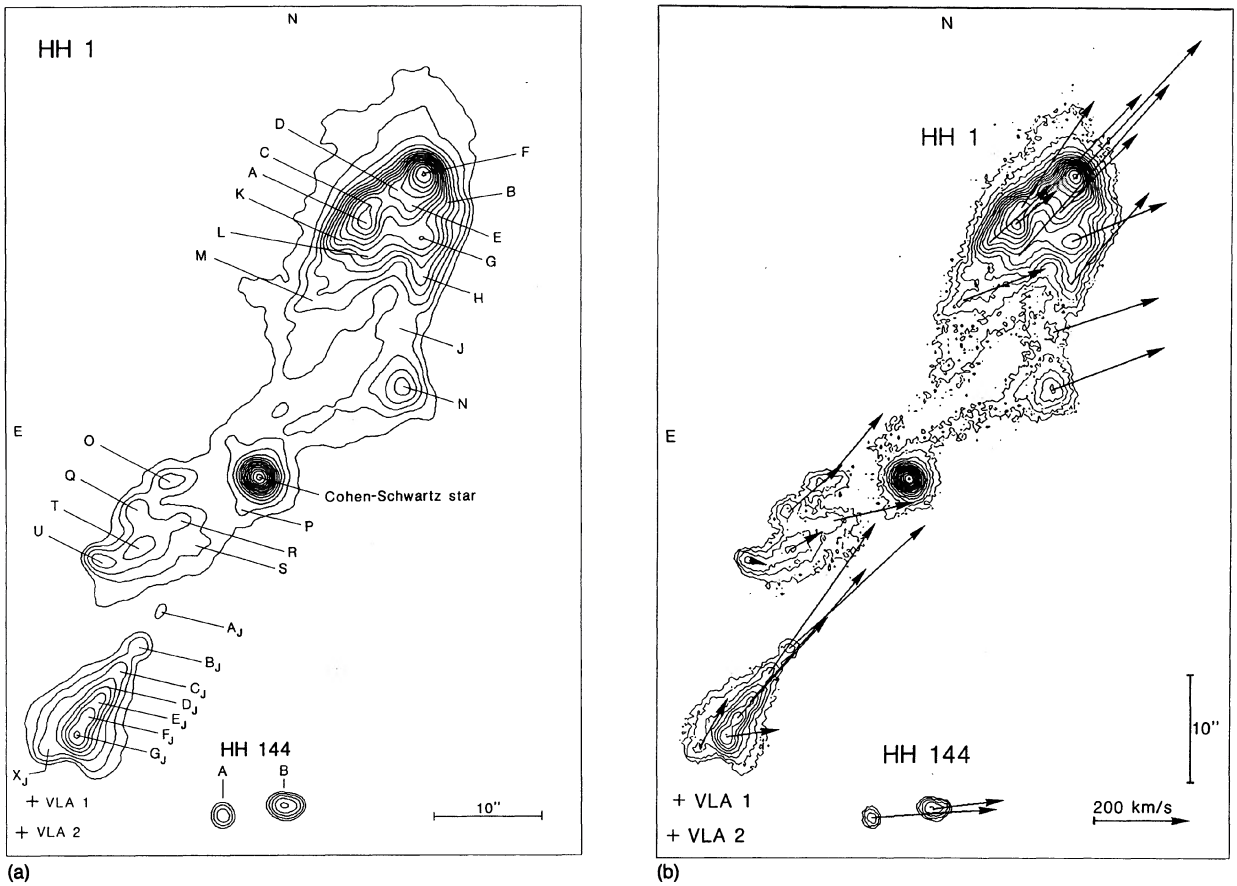

FIG. 5. (a) Designations of the condensations in the HH 1 region. (b) Proper motions of the condensations in the HH 1 region.

In the VLA1 jet tangential velocities ranging from 110 to 370 km s^{-1} were measured. These velocities increase with distance from the source. This increase is strongest between knot G_J and E_J, while it is small between knots E_J and B_J. Knots F_J to B_J move along the jet axis at an average position angle of 318°±5°. Knot G_J, however, shows a strong sideways deviation from this average direction of motion. In Sec. *3.1* we already discussed the possibility, that this knot might actually consist of two closely spaced knots—a northern one which is brighter in [S II] and a southwestern one, which is situated off the jet axis and is brighter in Hα and which may result from entrained ambient material. A different motion of these two knots would lead to a change in the shape of G_J as a whole and might cause the measured apparent sideways motion. Southeast of knot G_J there is another knot, X_J, which is also clearly off the jet axis and moves almost in jet direction at a similarly low tangential velocity as knot G_J. This knot may also result from entrained material or may be related to a more poorly collimated outflow component suggested in the H_2 images of Davis *et al.* (1994).

If we extrapolate the axis defined by the knots of the VLA1 jet towards HH 1 (assuming they move along a straight line) it is evident from Figs. 2 and 5 that this axis does not pass through the HH 1 apex, but is displaced in western direction and passes the bow shock approximately near knot H or B. Such a shift between jet and axis of symmetry of the bow shock has been observed also in other jet systems, e.g., for the HH 34 jet and its bow shock HH 34S (Bührke *et al.* 1988; Eislöffel & Mundt 1992). The reason for these shifts and displacements is not yet known. They could be due to bending of the flow by its environment or to a time-variable direction of ejection of the outflow from its source.

The proper motions of the knots in the HH 1 bow shock are shown in Fig. 5(b). These knots exhibit a surprising pattern of motion, since they seem to belong to two groups which are moving into two somewhat different directions. The northeastern group (group 1) consists of knots A, C, D, E, F, H, K, and L, which move at an average position angle of 317° (±5°), while the southwestern group (group 2) consists of knots G, J, M, and N, which move at an average position angle of 290° (±2°). The proper motion vectors of the group 1 knots have the same position angle as the knots in the VLA1 jet. Their tangential velocity is highest for knot F, the apex of the bow shock, with a value of 380 km s^{-1}, which is comparable to the highest jet tangential velocity of 370 km s^{-1}. It decreases along the wings of the HH 1 bow shock down to values of 100–200 km s^{-1}, as expected according to simple bow shock models (see also below). These results strongly suggest, that the group 1 knots indeed result from the VLA1 jet and hence belong to the flow from VLA1.

The knots in group 2 all have tangential velocities of about 200 km s^{-1}. The backwards projections of their proper motion vectors point east or southeast of the CS star. There

TABLE 2. Proper motions and tangential velocities of the knots in the HH 1 region.

Knot	v_{tan} ["/yr]	v_{tan} [km s^{-1}]*	PA [°]
A	0.050 ± 0.009	107 ± 19	308.4 ± 9.2
C	0.121 ± 0.015	258 ± 33	325.8 ± 6.7
D	0.128 ± 0.019	274 ± 40	316.3 ± 8.4
E	0.103 ± 0.022	221 ± 47	315.3 ± 12.2
F	0.178 ± 0.014	381 ± 29	317.5 ± 4.2
G	0.096 ± 0.010	206 ± 22	292.6 ± 6.5
H	0.111 ± 0.014	236 ± 31	319.1 ± 6.8
J	0.104 ± 0.025	222 ± 53	287.8 ± 12.6
K	0.079 ± 0.023	168 ± 48	313.0 ± 16.3
L	0.216 ± 0.020	463 ± 42	318.5 ± 5.5
M	0.083 ± 0.041	178 ± 88	290.8 ± 26.9
N	0.112 ± 0.018	240 ± 39	290.3 ± 7.7
O	0.085 ± 0.017	182 ± 37	319.2 ± 12.6
Q	0.067 ± 0.021	144 ± 46	312.0 ± 18.9
R	0.080 ± 0.017	171 ± 36	282.3 ± 8.7
T	0.034 ± 0.011	73 ± 24	300.2 ± 20.7
U	0.016 ± 0.036	35 ± 76	253.9 ± 75.2
B_J	0.173 ± 0.011	371 ± 24	311.5 ± 3.6
C_J	0.171 ± 0.018	366 ± 37	324.2 ± 5.6
E_J	0.165 ± 0.020	353 ± 42	318.4 ± 7.0
F_J	0.127 ± 0.013	271 ± 29	318.0 ± 5.6
G_J	0.051 ± 0.008	108 ± 18	277.7 ± 9.1
X_J	0.052 ± 0.026	112 ± 55	329.2 ± 18.8

* for a distance to HH 1 of 450 pc

we find another group of fainter knots *O*, *Q*, *R*, *T*, and *U*, which have a very similar average position angle of motion of 294° (though with a large scatter of ±26°). The velocity of these knots increases steadily from southeast to northwest, from close to the detection limit for the faint, diffuse knot *U* to values around 180 km s^{-1} for the northwestern knots *O* and *P*. Because of their positions and directions of motion most of these knots *G*, *J*, *M*, *N*, *O*, *Q*, *R*, and *T* seem not to belong to the highly collimated VLA1 jet. As is best seen on the H_2 and *K* band images of Davis *et al.* (1994) where knots *O*, *Q*, *R*, *T*, and *U* are all situated inside or at the walls of the cone-shaped cavity, which extends away from the VLA1 source. Therefore it may be possible that knots *O*, *Q*, *R*, *T*, and *U* belong to a lower collimation wind component in the outflow from VLA1 or could result from a time-dependent ejection direction of the outflow. Alternatively it seems likely that all knots *G*, *J*, *M*, *N*, *O*, *Q*, *R*, and *T* form an outflow of there own, which was suspected already by Strom *et al.* (1985) on morphological grounds. This outflow would be crossing the VLA1 jet at an angle of about 25° in projection onto the plane of the sky. It would be less collimated than the VLA1 jet and have a tangential velocity which is lower by about one-third. Its flow direction would be pointing exactly towards the faint knots visible in the upper left-hand corner of Fig. 1, which are believed to belong to HH 3 but for which unfortunately no proper motion measurements are available. Consequently we cannot verify whether they are moving in the same direction as the group 2 knots or whether they are eventually moving in the same direction as HH 3 (see Herbig & Jones 1981). Although the CS star is projected onto this possible outflow it is most probably not its source, because the proper motion vectors of both the knots southeast and northwest of it point into the same direction. They would indicate a source further southeast of knot *U*.

For four of the bright knots in HH 1 (knots *A*,*C*,*D*,*F*) proper motions were measured by Herbig & Jones (1981) on photographic plates. They had a dozen plates available with a total epoch difference of 20 yr, with which they achieved an accuracy comparable to ours. Within the measurement errors our measurements agree well with theirs. Only for knot *A* we find a position angle smaller by about 30°.

3.4 Proper Motion Measurements of HH 2

The designations of the individual knots in HH 2 are shown in Fig. 6(a). We adopted the designations by Herbig & Jones (1981) and Schwartz *et al.* (1993) and extended them according to our needs. Note that the knots called *A*1′, *A*2′, *A*3′, and *A*4′ here were called *A*1, *A*2, *A*3, and *A*4 by Schwartz *et al.* (1993) (but see the photometric history in Sec. *3.1* for a justification). Table 3 lists the proper motions for all measured knots in HH 2 and Fig. 6(b) shows the proper motion vectors.

Though at first glance HH 2 seems to have a very complex pattern of motion, several sections of HH 2 show some structure of common motion. Beginning at the "main" body of HH 2 the bright knots *A*′, *C*, and *H* are moving at tangential velocities of 110–330 km s^{-1} and an average position angle of 141° (±19°). These velocities range from average values seen in HH 2 to the fastest values measured in this object (with the exception of a few isolated and not very well defined condensations for which faster velocities have been measured). The average position angle coincides well with the counterdirection of the VLA1 outflow. Only condensation *H*2 shows a strong deviation from this general flow direction.

At the apex of HH 2 the moderately bright knot *L* is situated, the proper motion vectors of which are oriented in a similar direction as for the bright knots *A*′ and *H*. Its three leading condensations show, however, very low tangential velocities of about 60 km s^{-1}. Only for the less well-defined knot *L*4, which is moving upstream of the others, we measured a considerably higher tangential velocity of 220 km s^{-1}.

Downstream of the bright main body of HH 2, but upstream of the leading knots *L*, the two faint condensations *J*1 and *J*2 are situated. Their tangential velocities decrease from 130 km s^{-1} for the upstream one to 60 km s^{-1} for the downstream one; i.e., while the first knot is moving at the lower end of the range of velocities observed for the knots in the main body of HH 2, the second knot moves at a velocity similar to the condensations in knot *L* ahead of it.

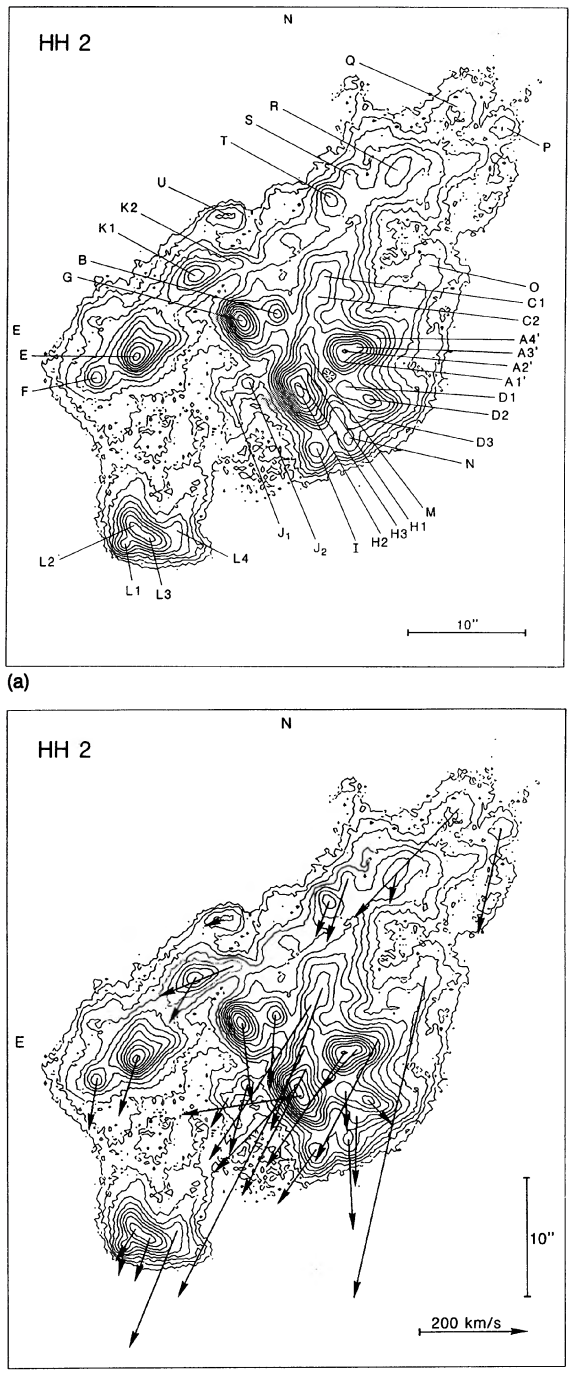

FIG. 6. (a) Designations of the condensations in HH 2. (b) Proper motions of the condensations in HH 2.

TABLE 3. Proper motions and tangential velocities of the knots in HH 2.

Knot	v_{tan} ["/yr]	v_{tan} [km s^{-1}]*	PA [°]
A2'	0.116 ± 0.015	249 ± 31	145.3 ± 8.5
A3'	0.053 ± 0.018	113 ± 38	137.3 ± 20.0
A4'	0.114 ± 0.042	244 ± 91	152.0 ± 20.9
B	0.060 ± 0.013	128 ± 28	175.8 ± 11.0
C1	0.126 ± 0.051	270 ± 109	159.9 ± 12.7
C2	0.156 ± 0.021	333 ± 45	146.4 ± 6.6
D1	0.032 ± 0.010	69 ± 22	182.0 ± 15.1
D2	0.030 ± 0.011	65 ± 24	222.9 ± 21.8
D3	0.057 ± 0.005	121 ± 10	178.5 ± 10.3
E	0.051 ± 0.014	109 ± 30	162.4 ± 11.3
F	0.043 ± 0.008	93 ± 18	170.7 ± 22.6
G	0.068 ± 0.009	145 ± 18	186.8 ± 8.2
H1	0.118 ± 0.032	253 ± 67	152.8 ± 9.5
H2	0.102 ± 0.015	219 ± 33	98.4 ± 5.3
H3	0.101 ± 0.015	216 ± 31	135.6 ± 8.3
I	0.054 ± 0.012	117 ± 25	144.4 ± 14.1
J1	0.028 ± 0.022	60 ± 47	148.9 ± 41.5
J2	0.061 ± 0.008	130 ± 17	165.2 ± 6.7
K1	0.044 ± 0.008	94 ± 18	148.9 ± 11.9
K2	0.066 ± 0.011	141 ± 24	111.4 ± 11.6
L1	0.024 ± 0.007	51 ± 16	165.9 ± 25.0
L2	0.029 ± 0.018	61 ± 38	147.5 ± 39.6
L3	0.035 ± 0.017	75 ± 37	161.5 ± 53.2
L4	0.102 ± 0.022	219 ± 47	157.2 ± 11.2
M	0.230 ± 0.033	491 ± 70	152.3 ± 5.9
N	0.075 ± 0.020	160 ± 43	183.0 ± 7.3
O	0.276 ± 0.033	589 ± 71	167.0 ± 6.2
P	0.088 ± 0.029	189 ± 62	167.5 ± 19.4
Q	0.125 ± 0.037	267 ± 79	135.7 ± 16.8
R	0.025 ± 0.013	53 ± 27	166.6 ± 16.5
S	0.054 ± 0.020	116 ± 43	161.1 ± 24.2
T	0.029 ± 0.017	62 ± 37	158.9 ± 22.1
U	0.016 ± 0.014	34 ± 29	109.0 ± 62.4

* for a distance to HH 2 of 450 pc

At the northeastern edge of HH 2 a row of moderately bright knots *K*, *E*, and *F* is moving at relatively small tangential velocities of about 90–140 km s^{-1}. Further upstream, this northwestern edge of HH 2 is defined by the faint knots *T*, *S*, and *R*, which are moving at similar or somewhat lower velocities (50–120 km s^{-1}). All these knots along the northeastern edge of HH 2 show a more southernly direction of motion (i.e., slightly "inward" towards the main body of HH 2) and therefore the average position angle (161°±7°) is 20° larger than for the knots in the main body. Knots *B* and *G*, which are situated midway at this side of HH 2 (but closer to the center) show a similar behavior. They have tangential velocities of about 130 km s^{-1} and move at position angles of 175° and 187°, i.e., practically south.

At the western edge of HH 2 a group of fainter knots *D*,*N*,*I* is situated. They have velocities in the range 65–160 km s^{-1}, which is similar to the knots along the northeastern edge of HH 2. The average position angle of motion of knots *D* and *N* is about 30° larger than for the knots in the main body. So they are moving slightly outwards in southwards direction.

Proper motions for eight of the bright knots in HH 2 were measured by Herbig & Jones (1981) on photographic plates. They had 28 plates available with a total epoch difference of 35 yr, from which they achieved an accuracy on average slightly better than ours. Both sets of measurements are not so easily comparable as in the case of HH 1, because we often measured several closely spaced knots, which they could only see as one entity. The overall agreement within the measurement errors, however, is good (for condensations $A2/3'$, B, $D2$, $C1/2$, and E). Real differences occurred for the faintest knot I measured by Herbig & Jones, where we measured only half the velocity, and for knot G, where we measured a 40° larger position angle. Note that the latter knot showed a change of shape during Herbig & Jones' measurements (see their Fig. 2 and compare images from 1971 and 1980) and was fading during our photometric monitoring. Also condensation H is known to undergo internal structural changes and hence the different position angle found for $H2$, compared to $H1$ and $H3$, is no surprise.

3.5 Proper Motion Measurements of HH 144 and 145

The designations of the individual knots in HH 144 and 145 are shown in Figs. 5(a) and 7(a). We adopted the designations by Reipurth *et al.* (1993). Table 4 lists the proper motions for all measured knots and Figs. 5(b) and 7(b) show the measured proper motion vectors.

For HH 144A and B we measured tangential velocities of 250 and 150 km s^{-1}, respectively, and a direction of motion towards position angle 275°. We found these tangential velocities to be smaller by about a factor of 2 and the position angles to be larger by 14° and 22°, respectively, compared to the recent measurements of Reipurth *et al.* (1993). (Note that our measurement errors for these knots are smaller by about a factor of 10.) Within their errors, however, both measurements agree. The high accuracy of our measurements allowed to determine the source of this outflow. Back projections of the proper motion vectors of both HH 144A and B passed along VLA2 to within 0.″5 or less, while they stayed away from VLA1 by at least 3″. In other words, while VLA2 is well within the 1σ error strip, VLA1 is well outside a 2.5σ error strip in both cases. On grounds of these new measurements we established that VLA2 is the source of the HH 144 outflow, as already suspected by Reipurth *et al.* (1993).

For HH 144H we measured a tangential velocity of about 200 km s^{-1}, which is comparable to HH 144A and B. HH 144H, however, does not move in the direction of the latter knots. As the HH 144 flow shows some kinks and bends off its axis, e.g., near knot D, it is not clear, if HH 144H belongs to this flow or not.

The knots in HH 145 all have very small tangential velocities, which are close to our detection limit of about 50 km s^{-1} for these faint, diffuse knots. HH 145E and HH 145C (the only knot in HH 145, which showed a significant proper motion) could also be part of the HH 144 flow because of their direction of motion, but limited accuracy does not allow a definitive statement. For the other knots in HH 145 no flow pattern is evident, which is not surprising given the measurements are at our detection limit. It is clear, however, that the proper motions of these knots are very small and especially that they are much smaller than the tangential velocities observed in knots HH 144A and B. This suggests that these knots might not belong to the HH 144 flow, as suspected by Reipurth *et al.* (1993) on morphological grounds, unless they are slowed down relicts from a former outflow episode.

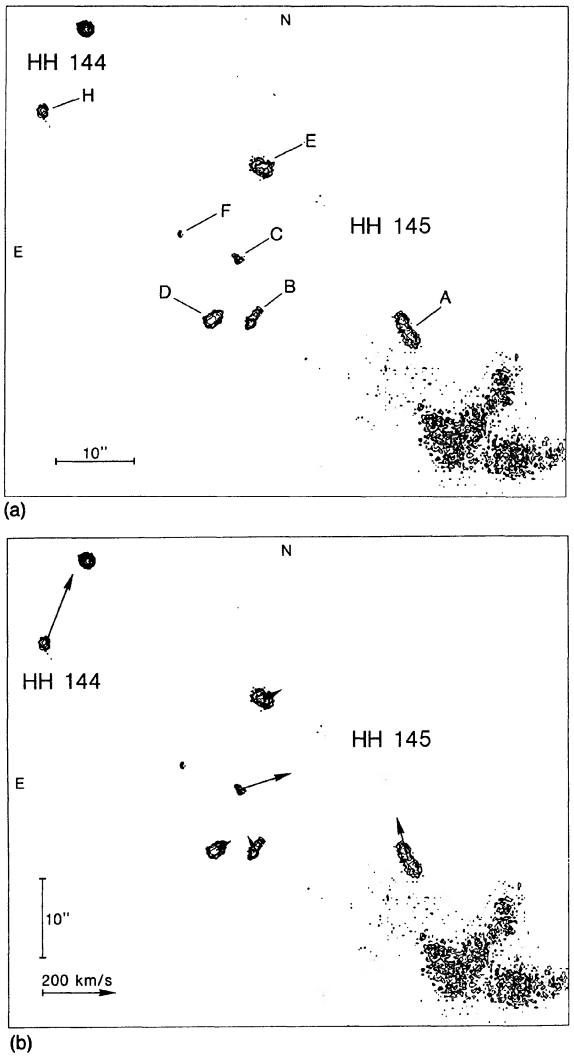

FIG. 7. (a) Designations of the condensations in HH 144 and HH 145 (see also Fig. 5). (b) Proper motions of the condensations in HH 144 and HH 145 (see also Fig. 5).

3.6 Proper Motion Measurements of HH 147

The designations of the individual knots in HH 147 is shown in Fig. 8 together with the measured proper motion vectors. The measured values of the tangential velocities and position angles are listed in Table 4.

HH 147 consists of two relatively extended, diffuse knots. HH 147A splits up into three components in lateral direction. Since this knot is rather diffuse, we measured the position of it as a whole, but rather did not try to measure positions for the individual components.

The HH 147 outflow points towards the south-west at a

TABLE 4. Proper motions and tangential velocities of the knots in HH 144, HH 145, and HH 147.

Knot	v_{tan} ["/yr]	v_{tan} [km s^{-1}]*	PA [°]
HH 144A	0.120 ± 0.009	256 ± 19	273.8 ± 3.8
HH 144B	0.066 ± 0.010	142 ± 22	276.8 ± 3.6
HH 144H	0.096 ± 0.020	205 ± 42	337.8 ± 6.0
HH 145A	0.057 ± 0.055	122 ± 118	374.4 ± 31.7
HH 145B	0.019 ± 0.022	42 ± 46	391.3 ± 43.6
HH 145C	0.070 ± 0.030	150 ± 64	286.9 ± 12.1
HH 145D	0.022 ± 0.014	48 ± 29	302.9 ± 36.9
HH 145E	0.016 ± 0.030	35 ± 65	288.2 ± 61.2
HH 147A	0.147 ± 0.068	315 ± 145	236.8 ± 38.2
HH 147B	0.093 ± 0.015	198 ± 31	221.2 ± 9.0

* for a distance to HH 144, HH 145 and HH 147 of 450 pc

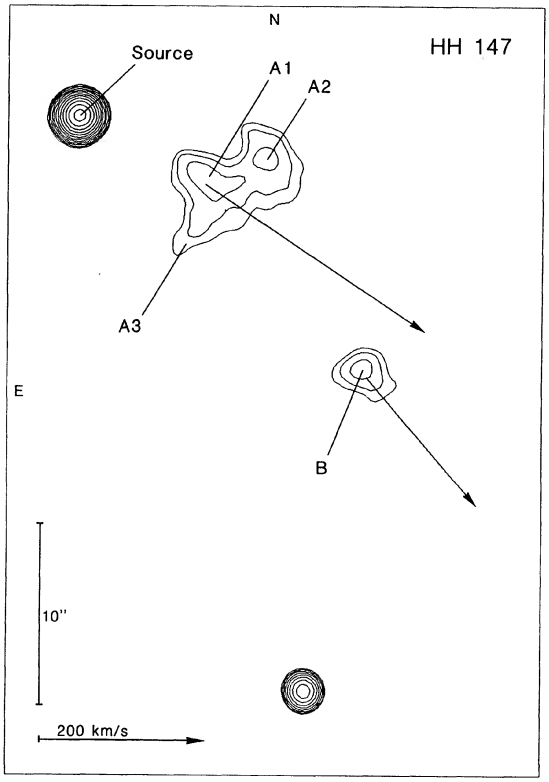

FIG. 8. Designations and proper motions of the condensations in HH 147.

position angle of about 230°. Its knots *A* and *B* move at the relatively high tangential velocity of 200–300 km s^{-1}. The backwards projections of their proper motion vectors lead to a star about 10″ northeast of HH 147A. This star, No. 3 of Strom *et al.* (1985), was classified as a T Tauri star by Strom *et al.* (1989). They report that its optical spectrum is of spectral type G5–G7 and that it exhibits strong [O I] and [S II] emission lines. They estimated a bolometric luminosity of 30 $L_{\odot}$. Recent observations by Corcoran & Ray (1994) showed that star No. 3 belongs to the rare type of T Tauri stars with a P Cygni profile in Hα. Its proximity to HH 147A, the direction of the proper motions of HH 147 and its spectroscopic properties make it most probable that star No. 3 is the source of the HH 147 outflow.

4. DISCUSSION

4.1 Structure and Kinematics of HH 1

Our proper motion measurements of knots in HH 1 basically confirm the idea that HH 1 is a relatively simple bow shocklike structure (moving in the plane of the sky) in which the largest velocities occur in the condensation *F*, which is the apex (the stagnation region of the bow shock) of HH 1. The knots in the wings of the bow shock (like *D*,*C*,*A*, etc.) show considerably smaller motion but still deviate only moderately from the direction of the flow of *F*. This could basically be recognized already in the proper motion measurements by Herbig & Jones (1981). These, as well as most spectroscopic results, are at least qualitatively compatible with the numerical predictions for a two-dimensional (time-dependent) bow shock model (Raga *et al.* 1988). Some not yet resolved difficulties have, however, been encountered when we tried earlier to interpret a fully two-dimensional image of the velocity dispersion distribution with this same model (Solf *et al.* 1991, see below). Nevertheless we feel that the agreements between observations and bow shock theory are sufficiently numerous and strong that there can be little doubt that HH 1 is basically a bow shock. The discrepancies between predicted and observed velocity dispersion are relatively large only in the immediate environment of knot *G*, a fact to which we will come back below.

Our present proper motion measurements cover 12 knots in HH 1 and its immediate environment [Fig. 5(b)]. Proper motions of four knots in HH 1 had been measured earlier by Herbig & Jones (1981). Our measurements include eight knots which lie in HH 1, excluding the somewhat problematic environment of HH 1G or the very far wings. These proper motions agree at least qualitatively with the predicted proper motions (Raga *et al.* 1988, their Fig. 6; and Böhm 1989) for a nonstationary bow shock model, if (in agreement with these papers) the following is taken into account. If we consider the observed proper motions simply as particle velocities with respect to the preshock gas then the observed velocities do not go to zero with the distance from the stagnation region as *fast as predicted* by the bow shock model. However, if we subtract from all the velocity vectors a velocity of about 100 km s^{-1} (which corresponds to the velocity of the slowest condensation *A*) then we get a result which agrees much better with the theory (Raga *et al.* 1988; see their Fig. 6). This means that we have assumed that HH 1 is a bow shock, which moves into a gas, which itself streams

away from the central star (VLA1) at a velocity of about 100 km s^{-1}.

This hypothesis is not only useful for a better theoretical explanation of the proper motions of the knots but it also strongly reduces the well-known discrepancy between the HH 1F velocity determined from the proper motion (380 km s^{-1}) and the bow shock velocity of about 200 km s^{-1} determined from emission line ratios (e.g., Noriega-Crespo *et al.* 1989). The outflow of matter in front of HH 1 is also compatible with the flow of only about 200 km s^{-1} of HH 1 matter relative to the matter in front as determined from the interpretation of line profiles in front of HH 1 as being due to dust scattering (Noriega-Crespo *et al.* 1991). Herbig–Haro objects which move into an already moving flow seem to be fairly common and have been discussed repeatedly in recent years (see, e.g., Hartigan *et al.* 1990; Eislöffel & Mundt 1994). For HH 1 the H_2 2.12 μm imaging by Davis *et al.* (1994) indicates that there is indeed matter in front of HH 1. These authors found faint, extended H_2 emission about 20″ northwest of the HH 1 bow shock.

In addition, we encountered the following (possibly minor) problem. Surprisingly there are four knots (*G*, *J*, *N*, and *M*), three of which are in the western wing of the bow shock, whose proper motion vectors point more towards the west than those of other knots (their position angles are about 290° instead of about 320°) and which therefore seem to deviate from the pattern of proper motions seen in the main part of HH 1. It is surprising that the four velocity vectors of these knots are all almost exactly parallel to each other. We note that this type of motion occurs, e.g., in the condensation *G* which lies in a region in which also a velocity dispersion, which deviates considerably from the velocity dispersion predicted for a bow shock model, was found (Solf *et al.* 1991). It looks as if (for some reason which is not yet understood) the well-ordered flow pattern of the HH 1 bow shock is perturbed in the southwestern part of the object. This seems to lead to a change in proper motions and in the radial velocity dispersion in this region. It is not clear whether the basic bow shock pattern is strongly disturbed by different physical conditions (e.g., by a drastic change in environmental density) or whether another independent HH outflow (which may not be directly related to HH 1) is simply projected on the southwestern part of HH 1. As discussed before, further support for an independent outflow is provided by the knots *O*, *Q*, *R*, *T*, and *U* southeast of the CS star, of which the proper motions vectors point in a similar direction as the knots in the extreme wings of HH 1. The situation is not clear, however, since there are also some arguments in favor of environmental effects, which could explain why the morphology of HH 1 in certain emission lines deviates so much from axial symmetry. Notable examples are the Hα and [O III]$\lambda\lambda$ 4959, 5007 images in Fig. 9, [Plate 30] where the eastern edge of HH 1 is much more prominent. There, the bow shock consists of a number of well-defined, bright knots interspersed with emission, while its western part is very diffuse and faint. That this asymmetry, especially in [O III], is not due to variable extinction across the bow shock is demonstrated by a comparison of the images in Fig. 9 with the H_2 2.12 μm images of Davis *et al.* (1994), which show that the eastern wing of the bow shock is also much more prominent at IR wavelengths.

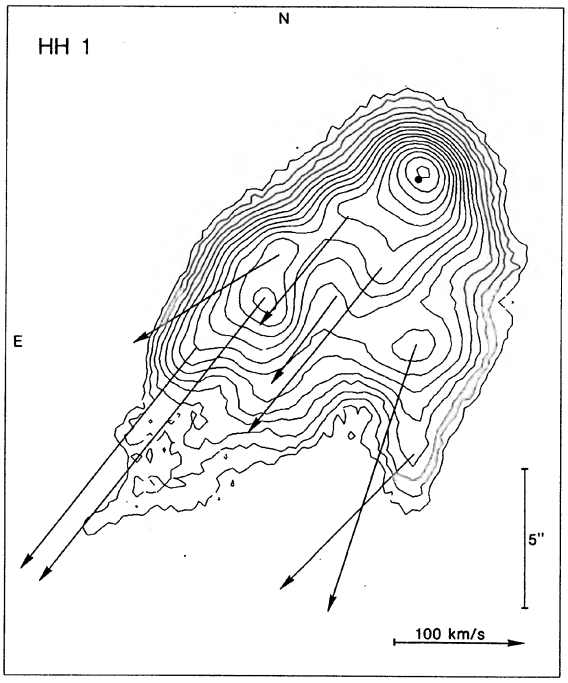

FIG. 10. Internal flow pattern in HH 1. The proper motion vector of condensation *F* at the stagnation point of the bow shock was subtracted to illustrate the relative motion of the condensations in the bow shock.

In Fig. 10 the proper motions in HH 1 relative to the stagnation region (HH 1F) have been plotted. In this case only the main part of HH 1 has been included, i.e., the proper motions in the extended bow shock wings are not shown. Consequently HH 1G is the only region with an unusual proper motion direction which is included in this diagram. In this type of presentation the relative proper motion of knot *G* does not look very unusual. Obviously the subtraction of the (large) stagnation velocity vector from the (smaller) individual velocity vectors leads to resulting vectors which all show relatively similar directions. The unusual proper motion directions of HH 1G and similar knots are obviously most clearly seen in Fig. 5(b).

In summary, we find that the proper motions inside and in the immediate environment of HH 1 are qualitatively compatible with the predictions for a bow shock model provided the following two complications are taken into account. We have to assume that the bow shock does not move into a gas which is at rest with respect to the central star, but rather into a gas which moves already in the direction of the HH 1 flow with a velocity of about 100 km s^{-1} (corresponding to the velocity of HH 1A, the slowest knot in HH 1). This assumption is compatible with spectroscopic information about HH 1, the recent H_2 2.12 μm imaging, and with our understanding of some other HH objects. We also have to recognize that the proper motion vectors in HH 1G and in three knots of the extended wings of HH 1 differ from the basic proper motion direction by about 30° and that these four velocity vectors all point in the direction of about 290°, possibly as a result of an

independent HH outflow or due to environmental effects. At least in the case of HH 1G this property seems to be related to an unusual velocity dispersion in the same area.

4.2 Outflow Activity in the Vicinity of HH 1/2

Until recently HH 1/2 was considered to be an isolated outflow, whose simple morphology and large brightness made the system a prototype outflow for comparisons of model calculations with observations. Now it turns out that HH 1/2 in fact is not an isolated outflow at all. In its neighborhood there are at least three other outflows with known sources: HH 144, HH 147, and HH 35 (source V380 Ori), and several more which are either located a bit further away or with yet unknown sources: HH 3, HH 36, HH 130, HH 145, HH 146 (and the possible outflow crossing HH 1). If all the latter six HH objects and the row of knots northwest of HH 1, seen only on the H_2 2.12 μm images of Davis *et al.* (1994), are indeed excited by different sources, then 11 young stellar objects produce outflows simultaneously in an area of about 1×1 pc^2. They form an "outflow cluster" similar to (albeit not as dense as) the cluster of outflows around HL Tau (Mundt *et al.* 1990).

As both radial and tangential velocities are available now for some of these outflows it is interesting to compare their flow directions and velocities. The HH 1/2 systems is situated very close to the plane of the sky, as evident from the small radial velocities ($\leqslant$20 km s^{-1}, see, e.g., Böhm & Solf 1985; Solf & Böhm 1991). While for HH 144 radial velocities $\leqslant$50 km s^{-1} were measured by Noriega-Crespo *et al.* (1993), for HH 147 A and B -10 and -60 km s^{-1}, respectively, were found by Corcoran & Ray (1994). The combination of these radial velocities with the tangential velocities given in this paper leads to orientations of the HH 144 and HH 147 outflows in the range of 0°–15° with respect to the plane of the sky. This means that these outflows, as well as HH 1/2, are seen practically without any projection effects. Hence the observed position angles of these outflows are very close to the real ones. These position angles (about 320° for HH 1/2, about 275° for HH 144, and about 230° for HH 147) are not aligned with each other nor with the local cloud magnetic field (146°, Strom *et al.* 1985), but fill a quadrant. The other above-mentioned outflows show a similar spread (although their directions of motion with respect to the plane of the sky are not yet clear). Thus many of the outflows in this small region seem not to follow the local cloud magnetic field, in contradiction to what was found for other outflows in L1641 by Reipurth (1989).

Our view of the real extent of the outflow activity in the HH 1/2 region still remains rather incomplete. The sources of the nearby HH objects, HH 145 and HH 146 (and the possible outflow crossing HH 1), are still unknown. Hardly any information on HH 36, HH 145, and HH 146 is available at all. More spectroscopic observations and proper motion measurements will be necessary to understand the kinematics in this outflow cluster.

4.3 Relations Between Proper Motions and Other Physical Properties of the Condensations in HH 1, HH 2, and the VLA1 Jet

The determination of the proper motions of a large number of clumps in a system whose axis of motion lies almost in the plane of the sky gives us useful information about the actual velocities of the clumps, provided the directions of the motions of the individual clumps do not deviate too strongly from the axis of the flow and the pattern motion of the knots are close to the true particle flow speed.

A study of the correlation of these tangential velocities with other known physical properties of the clumps seems to be useful because it may throw some light on the role which these clumps play in the hydrodynamics of the HH flow and it may also give us some information about the physical structure of the clumps.

Physical parameters which have been determined for at least a fraction of the clumps studied in this paper include the following. (1) The radial velocity dispersion (the information is usually restricted to the FWHM although in some cases the FWZI, i.e., the full width at zero intensity, or even detailed line profiles are also available). (2) The excitation as measured by the Hα/[S II] (6716+6731) line ratio; this line ratio can also be considered as an indicator of the shock velocity (see, e.g., Raymond 1979; Shull & McKee 1979, Hartigan *et al.* 1987). (3) The electron density. A problem with such a study is that the physical information mentioned is only available for a fraction of the clumps for which the proper motions have been measured. Moreover, our knowledge of such physical parameters is usually restricted to the relatively brighter clumps so that some selection effects are unavoidable. Nevertheless, we found it interesting to study the possible correlations between the velocities derived from proper motions, the excitation and radial velocity dispersion (as measured by the FWHM of the emission line profiles). We have not attempted to study the possible correlation between the proper motion and the electron density because information about the latter quantity was available only for a relatively small number of clumps.

A correlation between proper motions and radial velocity dispersion or excitation would be expected in case that the clumps of a HH object are due to instabilities of a single bow shock. Such a correlation would also be expected if the clumps are individual bow shocks moving with different velocities in the same direction.

In the following we shall discuss these correlations for HH 1, for HH 2, and for the jet of the system individually. Data on the radial velocity dispersion and the excitation have been taken from Solf & Böhm (1991), Solf *et al.* (1991), and Böhm & Solf (1992).

4.3.1 HH 1

As already mentioned above, this object has considerable similarity to a single bow shock (see, e.g., Choe *et al.* 1985; Böhm & Solf 1985; Hartigan *et al.* 1987; Raga *et al.* 1988), which is also evident from the images shown here in [S II]λλ 6716, 6731, Hα, and [O III]λλ 4959, 5007 (see Figs. 2, 5, and 9). However, the study of the two-dimensional distribution of

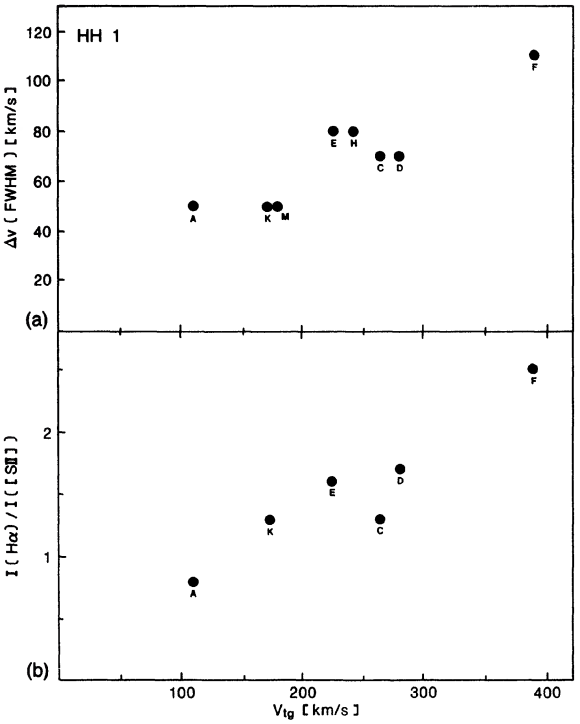

FIG. 11. (a) Tangential velocities vs radial velocity dispersion in HH 1. (b) Tangential velocities vs Hα/[S II]λλ 6716, 6731 ratio in HH 1. A linear correlation is found in both cases.

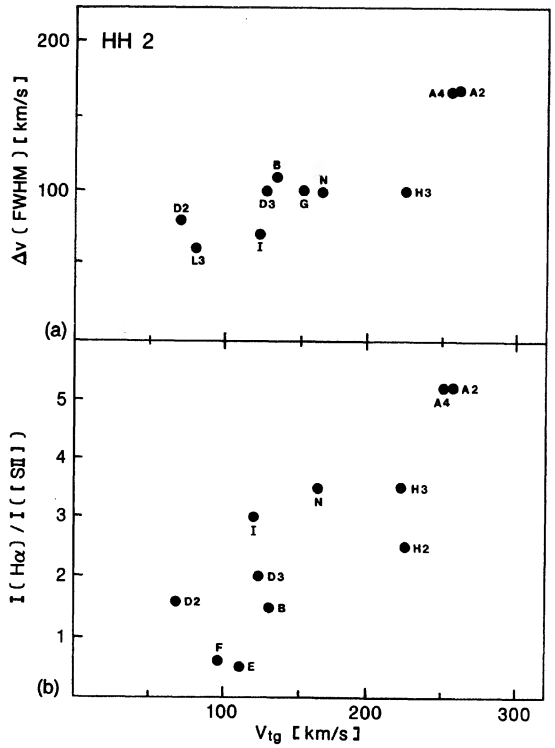

FIG. 12. (a) Tangential velocities vs radial velocity dispersion in HH 2. (b) Tangential velocities vs Hα/[S II]λλ 6716, 6731 ratio in HH 2. A linear correlation is found in both cases.

the radial velocity dispersion in HH 1 (Solf *et al.* 1991) has shown an unexpected but spatially rather limited feature in this distribution, which is not compatible with a bow shock model whose axis lies in the plane of the sky. In the environment of the faint condensation *G* near the western edge of HH 1 Solf *et al.* (1991) found an unexpectedly high velocity dispersion (which is almost comparable to that in the stagnation region of the bow shock). It is interesting that the clump *G* also shows an usual direction of its proper motion [see Fig. 5(b)]. While all the other clumps inside HH 1 show proper motions in directions about 315°–325° clump *G* moves in the direction 293°. This may be an indication that in this region light from an emission region, which is not a part of the bowshock (but possibly may belong to a different outflow) is superimposed on the image and that therefore we do not have to worry too much about the unusually large radial velocity dispersion in this region. For this reason we have excluded the HH 1G from the following study. Knots *J* and *N* show the same direction of the proper motion vector as *G* but they lie outside of the range for which we have information about velocity dispersion and excitation.

Consequently we consider the correlation between the proper motions and the excitation and velocity dispersion for the condensations *C*, *D*, *E*, *F*, *H*, *K*, and *M*. The correlations are shown in Figs. 11(a) and 11(b). We find a surprisingly good correlation between the proper motion and the radial velocity dispersion and between the proper motion and the excitation (measured by the Hα/[S II] ratio). Both the excitation and the radial velocity dispersion increase with increasing proper motion. This is to be expected if the axis of the motion is in the plane of the sky (see Herbig & Jones 1981) and if the observed clumps are parts of a single bow shock. A qualitatively similar correlation would also be expected if the clumps were individual small bow shocks moving in the plane of the sky in the same direction with different velocities.

4.3.2 HH 2

In this object the situation is somewhat similar to that in HH 1. We do, however, not have to exclude specifically clumps with unusual proper motions (like *G* in HH 1, see above). In HH 2 the proper motion directions in general show a fairly large scatter. The number of clumps included in this study is again limited because information about the radial velocity dispersion and the excitation is not available for all clumps for which the proper motion has been measured.

Figure 12(a) shows the correlation between proper motion and radial velocity dispersion, in which we have included the condensations *A2′*, *A4′*, *B*, *D2*, *D3*, *G*, *H3*, *I*, *L3*, and *N*. In Fig. 12(b) we consider the correlation between proper motion and excitation. In this case the condensations *A2′*, *A4′*, *B*, *D2*, *D3*, *E*, *F*, *H2*, *H3*, *I*, and *N* have been used. We would like to re-emphasize that we have always used all the condensations for which the appropriate information was available. Figures 12(a) and 12(b) show correlations in the same sense as HH 1: both the radial velocity dispersion and

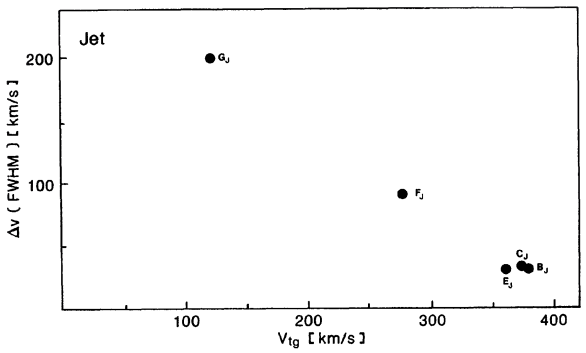

FIG. 13. Tangential velocities vs radial velocity dispersion in the VLA1 jet. Although only a few data points are available an anticorrelation is clearly indicated.

the excitation increase with increasing proper motions, leading to an analogous interpretation as in HH 1.

4.3.3 The jet

In this case we find an apparent correlation between proper motion and radial velocity which differs completely from that for HH 1 and HH 2. The radial velocity dispersion decreases drastically (and surprisingly) with increasing proper motion. Figure 13 shows the results. It is true (see Solf & Böhm 1991) that the blue wings of the emission lines from the jet are probably influenced by scattered light from the parts of the jet which are close to VLA1. However, it seems that the broad scattered line component mostly shows an intensity level of about 20% or less of the central line intensity (Solf & Böhm 1991) so that it is possible that the FWHM is not too strongly influenced by the light scattering.

It is interesting to compare the observed line widths with the observed opening angles. Note that for converging or diverging streamlines the observed line width is proportional to $\sin(\alpha/2)$, if the jet can be approximated by a homogeneously emitting cone with a full opening angle α [for details see Eq. (5) of Mundt *et al.* 1990]. As seen in Fig. 3 the jet converges between knots G_J and F_J with a full opening angle of about 15° and one would expect linewidths (FWHM) of about 100 km s^{-1} for a jet speed of 400 km s^{-1} for these two knots. Such a line width is observed for knot F_J, but for G_J it is about twice as large. A possible reason for this large line width in G_J could be entrainment of ambient material as already discussed above (see Sec. *3.1*). Between knots E_J and B_J the average full opening angle of the jet is about 3° and we would expect linewidths of about 20 km s^{-1}, consistent with the observations, except maybe for B_J, where the jet seems to "flare" and one would expect line widths about twice as large as observed. Since the observed linewidths can apparently be qualitatively explained by the effects of entrainment and converging/diverging streamlines, it has to be considered, whether the apparent correlation between the radial velocity dispersion and the tangential velocity is merely incidental.

4.3.4 Comparison with other results

A related correlation study using the Herbig & Jones (1981) proper motions and their own spectroscopy was carried out by Hartmann & Raymond (1984) for HH 1 and HH 2 only. They combined the data for these two objects and studied the correlation between tangential velocity and excitation (in their case measured by the intensity ratio [O III]λ5007/Hβ) and the correlation between the tangential velocity and the FWHM of the lines. Hartmann & Raymond (1984) do find correlations which are qualitatively similar but are less tight than those in our results. This can be attributed in part to our improved and more detailed data and in part to the fact that we have considered the correlations for HH 1 and HH 2 separately.

For HH 2 Cantó & Rodríguez (1986) have studied the correlation between the spatial velocities of the condensations and the electron densities. A corresponding study was not possible in our case because we do not yet have electron density data for many of the knots studied in this paper for the first time.

5. CONCLUSIONS

We have carried out a study of the proper motions of the condensations in the bright HH objects 1 and 2, and of the HH objects in their vicinity (HH 144, HH 145, and HH 147). We have undertaken photometric monitoring of the brighter condensations in HH 1 and 2. Furthermore we have deconvolved a [S II] image of HH 1 and the jet pointing towards HH 1, which was taken under good seeing conditions. The following results were obtained.

(1) The presented proper motions of HH 1 are compatible with the concept of HH 1 being a bow shock which is propagating into a medium, moving at about 100 km s^{-1} ahead of it. In the VLA1 jet tangential velocities steadily increasing from about 110 to 370 km s^{-1} were measured. The low tangential velocity of the jet knot G_J and its structural differences in Hα and [S II] suggest, that only part of the emission of this knot may be formed in the jet itself, while additional emission due to entrainment of ambient material may changes its morphology and kinematics. A number of knots situated between the VLA1 jet and the bow shock seem not to belong to the highly collimated jet, as indicated by their position and proper motion. They may result from the jets' interaction with an inhomogeneous environment, a lower collimation outflow component, a time-dependent ejection direction or even be part of an independent outflow, which incidentally is seen projected onto the VLA1–HH 1 flow. In HH 2 the proper motion measurements show a very complex kinematical structure, which is reminiscent of the complex morphology of this object. The measured tangential velocities vary mostly between 60 and 250 km s^{-1}.

(2) For HH 1 and 2 linear correlations were found between the tangential velocities of the condensations and their excitation and radial velocity dispersion, respectively. Both of the latter quantities increased with increasing tangential velocities. In HH 1 and 2 this is expected if the condensations are either individual bow shocks or parts of a single

bow shock. In the VLA1 jet, however, a surprising linear anticorrelation between tangential velocity and radial velocity dispersion is suggested.

(3) The deconvolved [S II] image of HH 1 (FWHM $=0\farcs55$) showed a wealth of detail in the HH 1 bow shock. Furthermore the knots in the VLA1 jet appear (just) resolved. The opening angle of the jet is found to be about 3° on average. Extrapolation from the visible knots to the source leads to an initial jet diameter of about $0\farcs4$. This is much larger than the diameter of $\leq 0\farcs1$ found by Rodríguez *et al.* (1990) from VLA observations, implying a larger opening angle close to the source.

(4) Photometric monitoring in the [S II] lines between 1987 January and 1993 April showed that many of the brighter condensations of HH 1 and 2 are variable. Most notable are the brightening of HH 2H by about 25%, the fading of HH 2C and G by about 20% and the strong variability of 10%–30% within only six years found for HH 1G, HH 2A′, B, D, and G. A comparison with observations carried out between 1946 and 1981 by Herbig (1969) and Herbig & Jones (1981) indicates that many condensations in the HH 1/2 system show substantial variability on time scales of years to several decades.

(5) The high accuracy of the proper motion measurements in HH 144 allowed to identify VLA2 as a most probable source of this outflow. Tangential velocities of about 150–250 km s^{-1} were measured for the brighter knots of this outflow. HH 145, near the end of the visible chain of knots of HH 144, showed only very small tangential velocities of mostly about 50 km s^{-1}. The investigation of the new outflow HH 147 northeast of HH 1 showed, that the T Tauri star No. 3 (Strom *et al.* 1985) probably is its source. Rather high tangential velocities of 200–300 km s^{-1} were measured for the the two diffuse knots in this flow.

(6) HH 1/2, HH 144, and HH 147 are all moving very close ($\leq 20°$) to the plane of the sky. These flows, as well as other nearby ones, however, appear not to be well aligned with respect to each other, nor with the local cloud magnetic field.

We are grateful to Alan Moorhouse, Ralf Poetzel, Tom Ray, and Alejandro Raga for taking images at our request or making them available from their archives and thereby allowing us to achieve the high accuracy of our proper motion measurements. We thank David Corcoran for communicating his spectroscopic data of HH 147 in advance of publication and Ulrich Hopp for procuring literature on the variability of HH 1/2 for us. Very useful discussions with Alberto Noriega-Crespo are gratefully acknowledged. K.-H.B.'s research has been supported by NSF Grant No. AST 91-14888. J.E. acknowledges support from the German Irish Research Fund and the Human Capital and Mobility Programme of the European Community under Grant No. ERBCHBGCT920205.

REFERENCES

Blondin, J. M., Fryxell, B. A., & Königl, A. 1990, ApJ, 360, 370
Blondin, J. M., Königl, A., & Fryxell, B. A. 1989, ApJ, 337, L37
Böhm, K. H. 1989, in Structure and Dynamics of the Interstellar Medium, edited by G. Tenorio-Tagle, M. Moles, and G. Melnick (Springer, Berlin), p. 282
Böhm, K. H., & Solf, J. 1985, ApJ, 294, 533
Böhm, K. H., & Solf, J. 1992, AJ, 104, 1193
Bührke, T., Mundt, R., & Ray, T. P. 1988, A&A, 200, 99
Cantó, J., & Rodríguez, L. F. 1986, RMxA, 13, 57
Choe, S.-U., Böhm, K. H., & Solf, J. 1985, ApJ, 288, 338
Cohen, M., & Schwartz, R. D. 1979, ApJ, 233, L77
Corcoran, D., & Ray, T. P. 1994, in preparation
Davis, C. J., Eislöffel, J., & Ray, T. P. 1994, ApJ (in press)
Edwards, S., & Snell, R. L. 1984, ApJ, 281, 237
Eislöffel, J., & Mundt, R. 1992, A&A, 263, 292
Eislöffel, J., & Mundt, R. 1994, A&A, 284, 530
Haro, G. 1952, ApJ, 115, 572
Hartigan, P., Morse, J. A., Heathcote, S., & Cecil, G. 1993, ApJ, 414, L121
Hartigan, P., Raymond, J., & Hartmann, L. 1987, ApJ, 316, 323
Hartigan, P., Raymond, J., & Meaburn, J. 1990, ApJ, 362, 624
Hartmann, L., & Raymond, J. C. 1984, ApJ, 276, 560
Harvey, P. M., Joy, M., Lester, D. F., & Wilking, B. A. 1986, ApJ, 301, 341
Herbig, G. H. 1951, ApJ, 113, 697
Herbig, G. H. 1969, in Nonperiodic Phenomena in Variable Stars, edited by L. Detre (Reidel, Dordrecht), p. 75
Herbig, G. H., & Jones, B. F. 1981, AJ, 86, 1232
Hirth, G. A., Mundt, R., Solf, J., & Ray, T. P. 1994, ApJ (in press)
Mundt, R., Brugel, E. W., & Bührke, T. 1987, ApJ, 319, 275
Mundt, R., Ray, T. P., Bührke, T., Raga, A. C., & Solf, J. 1990, A&A, 232, 37
Mundt, R., Ray, T. P., & Raga, A. C. 1991, A&A, 252, 740
Noriega-Crespo, A., Böhm, K. H., & Raga, A. C. 1989, AJ, 98, 1388
Noriega-Crespo, A., Calvet, N., & Böhm, K. H. 1991, ApJ, 379, 676
Noriega-Crespo, A., Garnavich, P., & Raga, A. C. 1993, in preparation
Pravdo, S. H., Rodríguez, L. F., Curiel, S., Cantó, J., Torrelles, M., Becker, R. H., & Sellgren, K. 1985, ApJ, 293, L35
Raga, A. C., Mateo, M., Böhm, K.-H., & Solf, J. 1988, AJ, 95, 1783
Raga, A. C., Mundt, R., & Ray, T. P. 1991, A&A, 252, 733
Raymond, J. 1979, ApJS, 39, 1
Reipurth, B. 1989, A&A, 220, 249
Reipurth, B., Heathcote, S., Roth, M., Noriega-Crespo, A., & Raga, A. C. 1993, ApJ, 408, L49
Rodríguez, L. F., Ho, P. T. B., Torrelles, J. M., Curiel, S., & Cantó, J. 1990, ApJ, 352, 645
Schwartz, R. D., *et al.* 1993, AJ, 106, 740
Shull, M. J., & McKee, C. F. 1979, ApJ, 227, 131
Solf, J., & Böhm, K. H. 1991, ApJ, 375, 618
Solf, J., Raga, A. C., Böhm, K. H., & Noriega-Crespo, A. 1991, AJ, 102, 1147
Strom, S. E., *et al.* 1985, AJ, 90, 2281
Strom, K. M., *et al.* 1989, ApJS, 71, 183

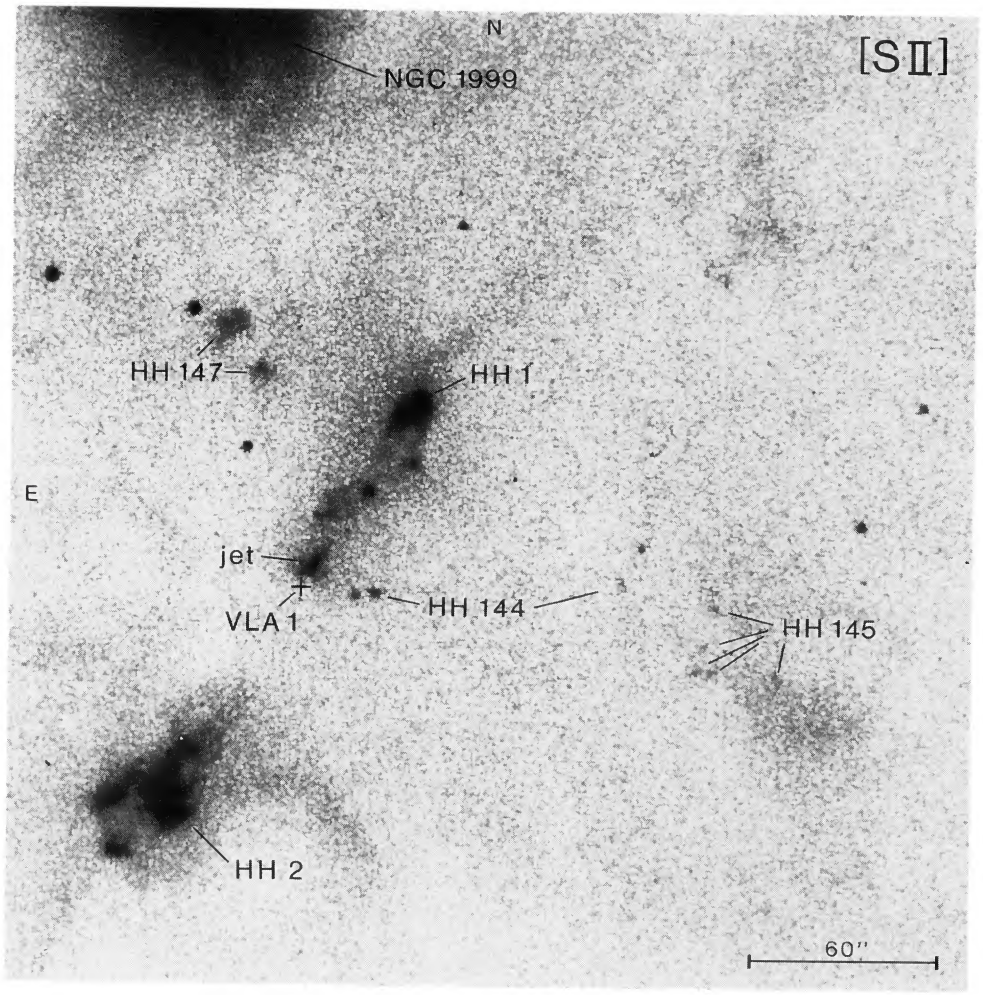

FIG. 1. Overview over the HH 1/2 region. HH 1 and 2 are the brightest Herbig–Haro objects in this image, which was taken through a [S II]λλ 6716, 6731 filter. A number of other HH objects in their vicinity are marked (HH 144, HH 145, HH 147). Several additional faint and diffuse HH knots in the upper right of this image are thought to belong to HH 3, which itself is only partly seen at the upper (right-hand) border of this image.

Eislöffel *et al.* (see page 1043)

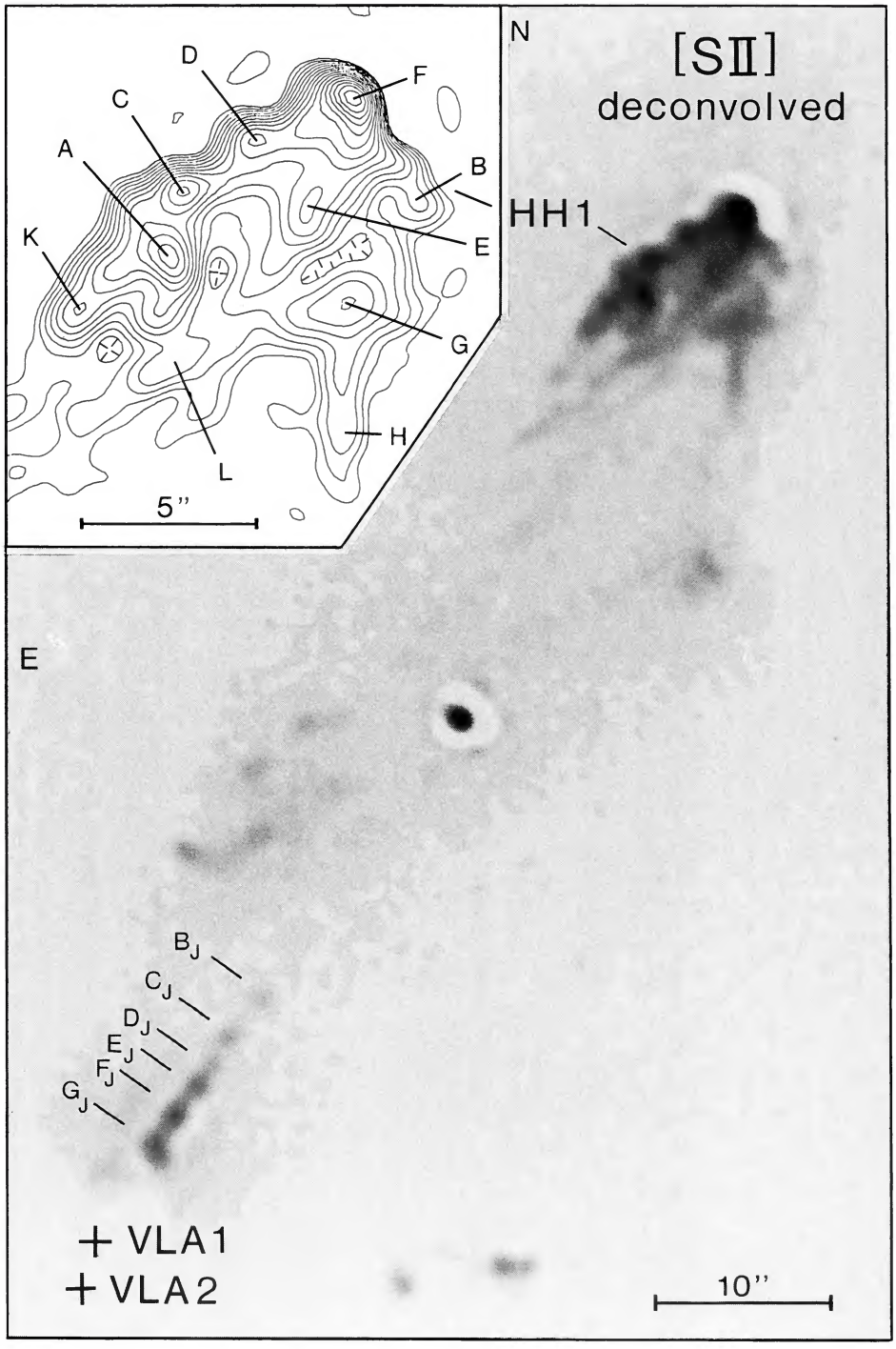

FIG. 2. High-resolution [S II] image (FWHM=0.″55) of the region between VLA1 and HH 1. It was deconvolved with the Richardson–Lucy algorithm using 40 iteration steps. The inset shows a contourplot of the HH 1 bow shock. A wealth of structural detail is seen in this image.

Eislöffel *et al.* (see page 1044)

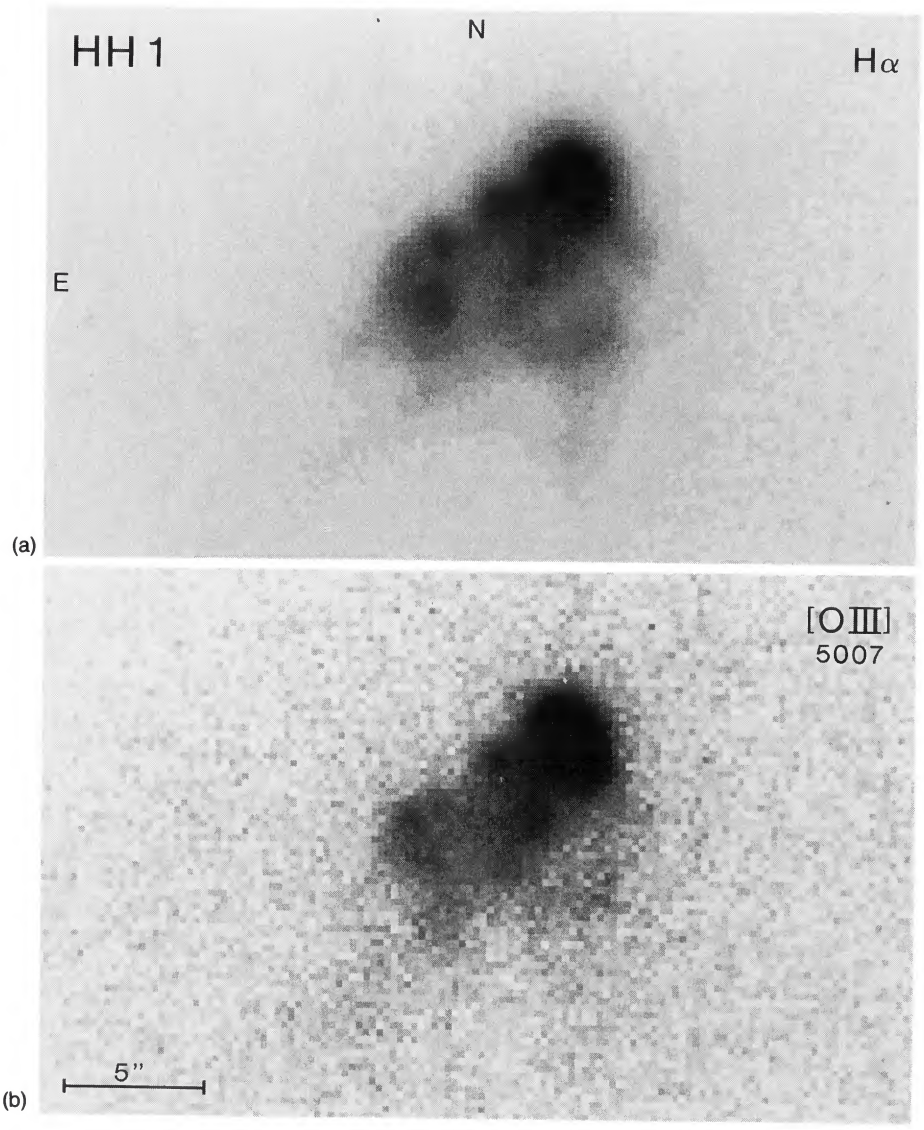

FIG. 9. (a) HH 1 taken through an Hα filter. (b) HH 1 taken through an [O III]$\lambda\lambda$ 4959, 5007 filter. The asymmetric morphology of the bow shock is evident on both images: while the eastern part of the bow shock consists of a number of well-defined bright knots interspersed with emission, the western part is faint and very diffuse.

Eislöffel *et al.* (see page 1051)

THE ASTRONOMICAL JOURNAL

FOUNDED BY B. A. GOULD
1849

LUME 108 **September 1994~No. 1664** *NUMBER 3*

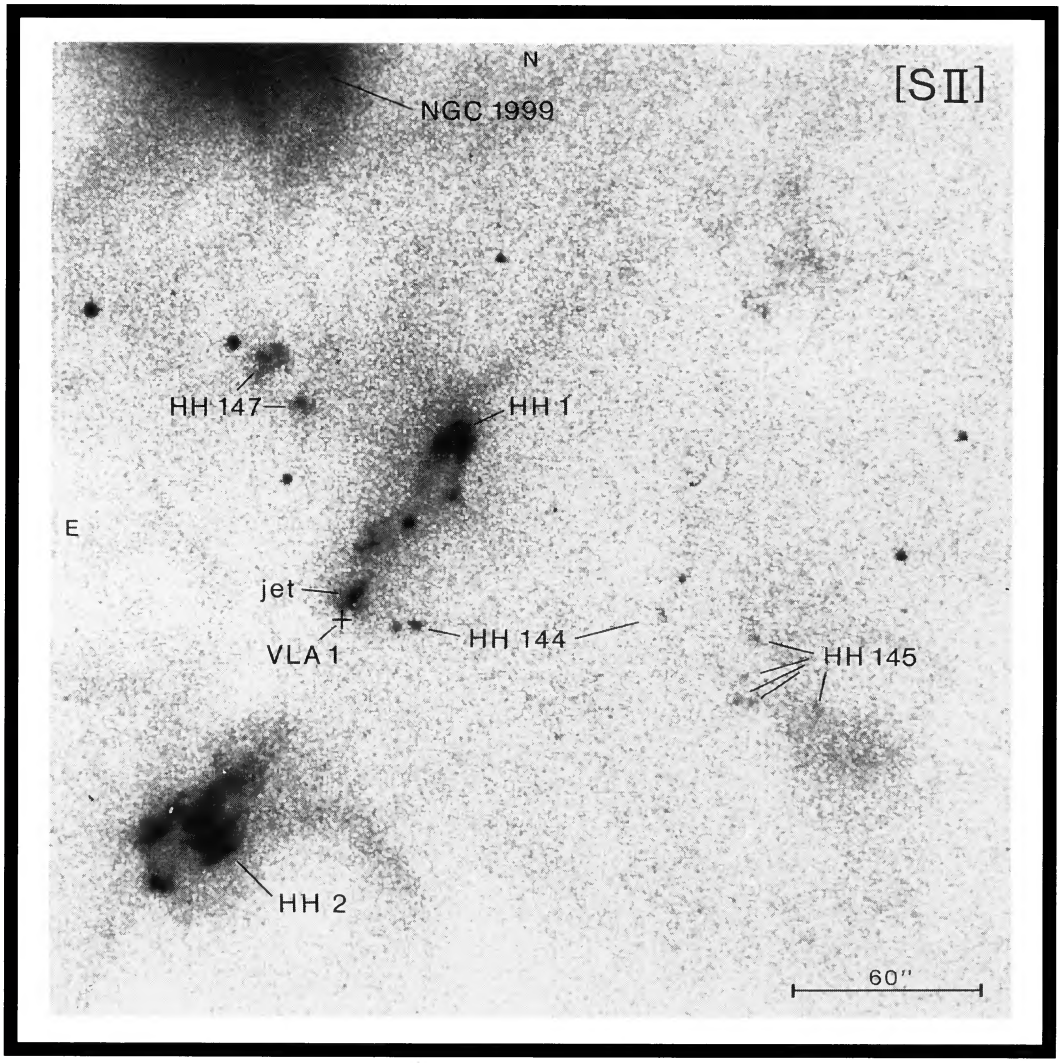

(See Page 1042)

Published for the
AMERICAN ASTRONOMICAL SOCIETY
by the
AMERICAN INSTITUTE OF PHYSICS